Journal of Magnetic Resonance **146,** 311–320 (2000)
doi:10.1006/jmre.2000.2138, available online at http://www.idealibrary.com on IDEAL®

PATROS—A New MAS Exchange Method Using Sideband Separation: Application to Poly(*n*-butylmethacrylate)

D. Reichert,*[,1] G. Hempel,* Z. Luz,† P. Tekely,‡ and H. Schneider*

**Department of Physics, NMR Group, University of Halle, Friedemann-Bach-Platz 6, 06188 Halle, Germany; †Chemical Physics Department, The Weizmann Institute of Science, Rehovot 76100, Israel; and ‡Laboratoire de Méthodologie RMN, UPRESA CNRS 7042, Université Henri Poincaré, Nancy 1, 54506 Vandoeuvre-lès-Nancy, France*

Received January 25, 2000; revised June 6, 2000

The tr-ODESSA method (Reichert *et al., J. Magn. Reson.* 125, 245 (1997)), which is a 1D MAS experiment designed to monitor spin exchange involving both equivalent and inequivalent sites, is extended to situations where the spectrum consists of several spinning side band (ssb) manifolds with small chemical shift anisotropies. To increase the spectral resolution in such situations, the tr-ODESSA sequence is combined with that of PASS to a single experiment, which we term PATROS. In this hybrid experiment, magnetization transfer is monitored by the tr-ODESSA part, while the increase in resolution is provided by the separation of the ssb according to their order, during the PASS part. We demonstrate the feasibility of the method on a standard solid dimethylsulfone (DMS) sample and then apply it to monitor separately the ultraslow motions of the main- and side-chains in the polymer poly(*n*-butylmethacrylate). Theoretical expressions for the ssb intensities in PATROS experiments are derived and the merits and limitations of the method are discussed.

Key Words: **1D-MAS exchange spectroscopy; tr-ODESSA; PASS; DMS; poly(*n*-butylmethacrylate).**

1. INTRODUCTION

MAS NMR exchange spectroscopy has proved to be a very powerful tool for the investigation of ultraslow (on the NMR time scale) dynamic processes, i.e., processes with rate constants of the order of 0.1 to 10^3 s^{-1} (*1*). Such slow processes are quite common in amorphous polymers and many other condensed matter systems (*2–4*). Their nature and rates play an important role in determining the macroscopic and microscopic properties of the systems, for example, the strength of construction polymers (*5, 6*) and the structure–function relationships in biopolymeres (*7, 8*). The main power of the ultraslow dynamic NMR methods lies in their ability to determine the characteristic rates and mechanisms of these motions and in their ability to identify the molecular segments at which the motions occur.

Because of its common occurrence in organic materials, carbon-13 is most often the nucleus of choice for such NMR investigations. Its low natural abundance limits, however, its general applicability to samples with favorable NMR properties, i.e., relatively intense signals and short relaxation times. In particular, 2D-exchange experiments (*9–11*) are often not practical for polymeric systems, due to low sensitivity and the consequent forbiddingly long measuring time. A practical solution to this problem is the application of the much less time consuming 1D Magnetization Transfer (MT) methods. Several such methods have been proposed (*12, 13*), but they are usually limited to monitoring exchange between inequivalent nuclei, and they are not suitable for studying exchange between congruent sites belonging to the same group of equivalent nuclei. By congruent nuclei we mean nuclei that have identical principal values of the chemical shift (CS) tensors, but their principal axes are rotated with respect to each other. For many systems exchange between equivalent sites are of major interest, since they reflect the more common situation of jumps between symmetry related sites, as in molecular crystals, or jumps between sites with similar isotropic CS, but different orientations of the anisotropic CS tensors, as in polymeric chains. Such exchange processes can still be studied using special experiments in which a selective nonequilibrium polarization is induced within the spinning side band (ssb) manifolds of the exchanging species. Experiments belonging to this category are the EIS (*14*), the ODESSA (*15*), and the time-reverse ODESSA (tr-ODESSA) (*16*). In the first of these experiments the ssb (except for the center band) are "canceled" by a TOSS sequence, while in the latter two they are alternatively polarized by a fixed delay of half a rotation period, $T_R/2 = 1/(2\nu_R)$, during the preparation period. The redistribution of the polarization within the ssb manifolds due to spin exchange and T_1 relaxation, as a function of a variable mixing period τ_m, is then monitored during the detection period. Among these methods the tr-ODESSA is particularly favorable; the EIS is very sensitive to the performance of the TOSS sequence, while the ODESSA yields phase distortions when there is more than one set of equivalent nuclei in the spectrum. Very recently, a modification of this method was proposed (*17*)

[1] To whom correspondence should be addressed. E-mail: reichert@physik.uni-halle.de.

1090-7807/00 $35.00

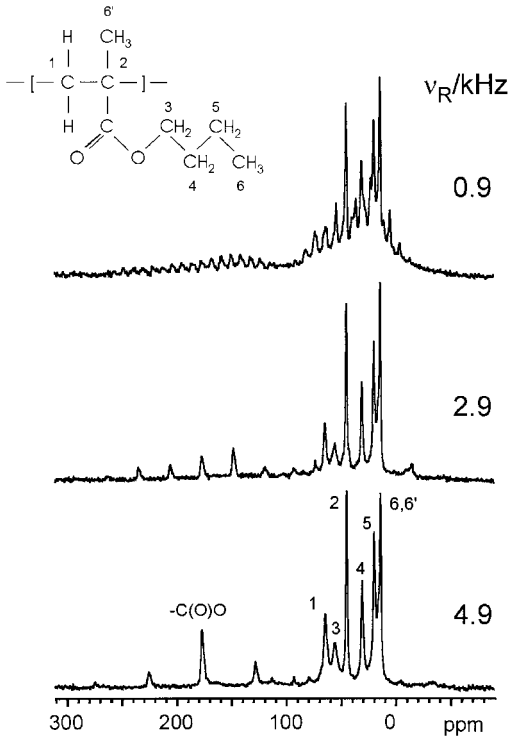

FIG. 1. Carbon-13 CPMAS spectra of Poly(*n*-butylmethacrylate) PBMA recorded at the indicated spinning frequencies, ν_R. One hundred twenty-eight scans with a repetition time of 1.5 s and a CP contact time of 2 ms were accumulated. $t = 25°C$. The insert depicts the structural unit of PBMA and the numbering system used. The peak assignment is given in the bottom spectrum.

where only one ssb manifold is excited, thus solving the phase distortion problem. On the other hand, in the tr-ODESSA experiment all ssb manifolds can be phased to pure absorption and will remain so if the exchange involves equivalent sites only. The experiment is also quite robust toward artifacts. The method was successfully applied to study spin exchange in a number of molecular solids and polymeric systems (*8, 18, 19*).

In tr-ODESSA, the spin exchange between congruent nuclei is manifested in different intensity decays of the different ssb. To obtain accurate kinetic results, it is necessary to work under conditions where there are several intense ssb of the same manifold. For aromatic and carbonyl carbons, which are characterized by a large CS anisotropy, the spectrum usually exhibits a sufficient number of ssb even at moderately fast spinning rates. However, for aliphatic carbons, whose CS anisotropy is small, it is often necessary to spin at very low frequencies in order to obtain sufficiently intense ssb. The situation is particularly difficult when one wants to study molecular dynamics in polymers consisting of hydrocarbon chains with several inequivalent aliphatic carbons. On slow spinning, one quickly runs into the problem of overlapping ssb belonging to different carbon manifolds. Figure 1 demonstrates the problem for the carbon-13 MAS spectrum of the amorphous polymer, Poly(*n*-butylmethacrylate) (PBMA). The spectrum at a spinning frequency of $\nu_r = 4.9$ kHz exhibits well-resolved signals due to carboxyl carbon (and its ssb) at 178 ppm, and the seven aliphatic carbons (see structural formula inserted in the figure) in the range 15 to 70 ppm. In principle, tr-ODESSA measurements of these carbons could provide separate information on the motion of the backbone, as well as that of the side chains. However, at a spinning frequency of 4.9 kHz the signals due to the aliphatic carbons do not exhibit ssb and they cannot therefore be used for dynamic measurements by tr-ODESSA method. The problem can be overcome by recording spectra at much slower spinning rates. Such a ssb-rich spectrum is shown at the top of Fig. 1, which was recorded at $\nu_r = 900$ Hz. At this spinning frequency there are ample ssb; however, there is also excessive overlap between those belonging to the different carbons, rendering accurate intensity measurements quite impossible.

To solve this problem and make dynamic measurements possible, we propose to combine the tr-ODESSA experiment with a pulse sequence capable of removing the spectral overlap between the ssb. Such a sequence is the PASS (Phase Adjusted Spinning Sidebands) originally proposed by Dixon (*20, 39*) and subsequently modified and extended to two-dimensions by Spiess and co-workers (*22, 23*) and by Levitt and co-workers (*24–27*). The PASS pulse sequence is shown in Fig. 2b. This experiment, on its own, results in a separation of the 1D spectrum according to the order of the ssb in a second dimension, thus removing the overlap between them. The combined *PASS-tr-ODESSA* sequence is shown in Fig. 2c. We accordingly term it PATROS. We emphasize again that the method removes overlap between ssb belonging to different carbons, but it does not resolve overlapping signals of the same order.

The theory of PATROS is outlined in Section 2, while in Section 3, the method is demonstrated on the model compound Dimethylsulfone (DMS). Finally, in Section 4, we apply it to the aliphatic carbons of the PBMA polymer.

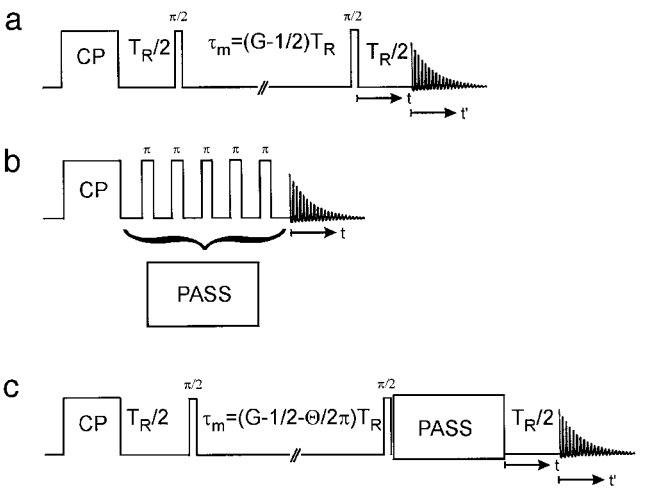

FIG. 2. Pulse sequences of (a) tr-ODESSA, (b) PASS, and (c) PATROS. For simplicity, only the channel of the *X* nucleus is shown. Proton decoupling is applied throughout, except during the mixing period.

2. THEORY

To derive an expression for the time domain (fid) signal of the PATROS experiment, it is convenient to first recall the equations for the separate MAS, tr-ODESSA, and PASS experiments. We then combine the latter two sequentially to create the 2D signal of the PATROS experiment.

The MAS fid of $I = \frac{1}{2}$ nuclei, subject to an anisotropic CS Hamiltonian is (*28*),

$$\begin{aligned} fid(t) &= e^{-(t/T_2)} e^{i\omega_0\sigma_{iso}t} e^{i\int_0^t \omega(t')dt'} \\ &= e^{-(t/T_2)} e^{i\omega_0\sigma_{iso}t} e^{i\Phi(t)} e^{-i\Phi(0)} \\ &= e^{-(t/T_2)} e^{i\omega_0\sigma_{iso}t} f(\omega_R t + \gamma)\, f^*(\gamma). \end{aligned} \quad [1]$$

Explicit formulas for the f functions in terms of the elements of the CS tensor, as well as some of their more important properties, can be found in the earlier literature (*1*, *16*, *29*, *30*). Equation [1] can be expanded into

$$fid(t) = e^{-(1/T_2)} e^{i\omega_0\sigma_{iso}t} \sum_M e^{iM\omega_R t} I_M, \quad [2]$$

where the I_M are complex intensities. When integrated over the angles α, β, and γ of an isotropic powder they yield the Herzfeld-Berger ssb intensities (*31*). We now use Eq. [1] in a stepwise manner to construct the fid signal of the tr-ODESSA experiment (Fig. 2a),

$$\begin{aligned} M_{ij}^{trO}(t) = {} & e^{-((T_R/2)/T_2)} e^{-i\omega_0\sigma_{iso}^j (T_R/2)} f^j(\gamma)\, f^{*j}(\pi + \gamma) \\ & \times e^{-(t/T_2)} e^{i\omega_0\sigma_{iso}^i t} f^{*i}(\pi + \omega_R\tau_m + \gamma) \\ & \times f^i(\pi + \omega_R\tau_m + \omega_R t + \gamma). \end{aligned} \quad [3]$$

Here, $M_{ij}^{trO}(t)$ is the contribution to the transverse magnetization from those nuclei that at the beginning of the mixing period were at site j and at its end at site i. The end of the first line in Eq. [3] corresponds to the magnetization just before the mixing period, assuming that the antiecho combination of cos and sin components was taken (*16*). During the mixing period, at which the magnetization is in Zeeman order and therefore not precessing, the nuclei may jump from site j to site i. Then, after the detection pulse, the magnetization evolves as described in the second line of Eq. [3], where we have neglected for the moment the longitudinal relaxation during τ_m. To obtain real spin exchange effects and well-phased spectra, we apply the condition of a time-reversed mixing period, $\tau_m = (G - \frac{1}{2})T_R$ (G being an interger) and start the signal acquisition at $T_R/2$ after the detection pulse. The term "time-reversed" was adapted from the phase sensitive 2D-MAS experiment, where it served to reverse the sign of t_1 in the indirect dimension (*11*). Equation [3] then becomes (*16*)

$$\begin{aligned} M_{ij}^{trO}(t') = {} & e^{-((T_R+t')/T_2)} e^{i\omega_0(\sigma_{iso}^i - \sigma_{iso}^j)(T_R/2)} e^{i\omega_0\sigma_{iso}^i t'} \\ & \times \sum_N e^{iN\omega_R t'} \sum_M (-1)^{(M-N)} I_{MN}^{ij}, \end{aligned} \quad [4]$$

where we have expanded the f functions as in Eq. [2] and integrated over α, β, and γ. The I_{MN}^{ij} in this equation correspond to the MN, ij cross peaks in the 2D-MAS exchange experiment (*29*). Finally, the overall time domain signal is given by

$$S(t', \tau_m) = \sum_{ij} P_{ij}(\tau_m)\, M_{ij}^{trO}(t'), \quad [5]$$

where $P_{ij}(\tau_m)$ is the fractional probability of finding a probe nucleus at site j before and at site i after the mixing period,

$$P_{ij}(\tau_m) = (e^{K\tau_m})_{ij} P_j(0). \quad [6]$$

$P_j(0)$ is the equilibrium populations of site j and K is the exchange/relaxation matrix; i.e., it includes the exchange and longitudinal relaxation terms. For a pair of congruent sites, the intensity of the ssb of order N, $I_N(\tau_m)$ becomes (*16*)

$$\begin{aligned} I_N(\tau_m) &= (A_N + B_N e^{-2k\tau_m}) e^{-(\tau_m/T_1)} \\ A_N &= \frac{1}{2}(I_N^{11} + I_N^{12}) \quad B_N = \frac{1}{2}(I_N^{11} - I_N^{12}) \\ I_N^{11} &= I_N^{22} \quad I_N^{12} = I_N^{21}, \end{aligned} \quad [7]$$

where the I_N^{ij} can be calculated from the so-called f functions as described in Refs. (*11*) and (*29*).

We next discuss the PASS experiment. Its pulse sequence, shown in Fig. 2b, consists of a train of five, properly timed and phase cycled, π-pulses (*24*). For each group of equivalent nuclei the experiment leads to an output signal of the form

$$M^{PASS}(t) = e^{-((T^{PASS}+t)/T_2)} e^{i\omega_0\sigma_{iso}^i t} f^*(\gamma + \Theta)\, f(\omega_R t + \gamma), \quad [8]$$

where Θ is the "pitch" (phase shift) induced by the sequence. This phase shift is the essence of the PASS experiment and can be set to any desired value by adjusting the timing of the PASS sequence (*24*). The period T^{PASS} is the total length of the PASS sequence, which in the five π-pulse version is fixed and is independent of Θ. Expanding the right-hand side of Eq. [8] as before, one obtains

$$M^{PASS}(t) = e^{-((T^{PASS}+t)/T_2)} e^{i\omega_0\sigma_{iso}^i t} \sum_M e^{iN\omega_R t} e^{-iN\Theta} I_N^i. \quad [9]$$

Thus the PASS spectrum is identical to that of MAS (Eq. [2]), except that all ssb manifolds exhibit a linear phase shift, $N\Theta$, centered at their respective isotropic frequencies. This means that they cannot be phased simultaneously to pure

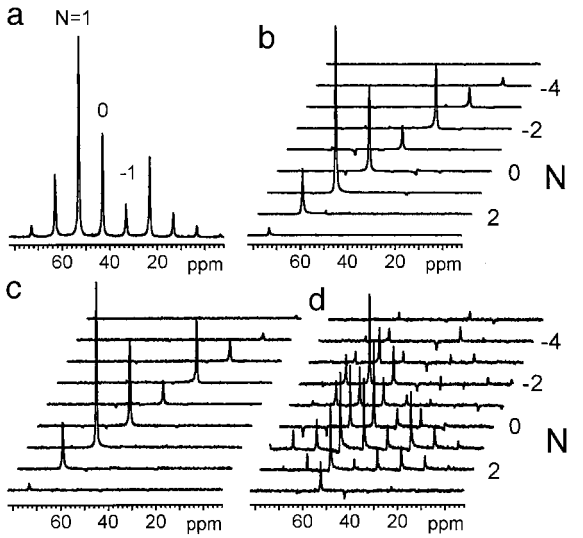

FIG. 3. (a) Carbon-13 MAS, (b) PASS, and (c and d) PATROS spectra of DMS. Two hundred fifty-six scans with a repetition time of 1 s were accumulated in (a) and for each increment in (b)–(d). The CP contact time was 0.2 ms. In (b)–(d), 16 Θ-increments were recorded. The nominal mixing period in (c) and (d) was 1 ms. In (c) τ_m was set to the PATROS condition $\tau_m = (G - \frac{1}{2} - \Theta/2\pi)\, T_R$, while in (d), it was intentionally set, incorrectly, to the tr-ODESSA condition $\tau_m = (G - \frac{1}{2})\, T_R$. $t = 25°C$, $\nu_R = 1$ kHz, $G = 2$.

absorption. By incrementing Θ in equal steps of $2\pi/n$ (n being the number of observed ssb), we obtain a sequence of fid's, which are phase modulated according to the order of the ssb. Two-dimensional FT with respect to t and Θ yields a 2D-spectrum resolved in the second dimension according to the order of the ssb. Each $M\nu_R$ slice in the indirect dimension of this spectrum consists, for each type of nuclei, of a single peak at $\nu_0\sigma^i_{iso} + N\nu_R$. Since there is no relaxation decay in this dimension and the phase shift is linear in the order of the ssb, it is sufficient to acquire, within a single rotation period, only as many Θ increments (n) as the observed number of ssb. To make use of the standard FFT algorithm, we need to increment the Θ's at equal steps and set their number equal to $n = 2^L$ (L integer). It should be noted that the original PASS sequence (*20, 39*) consists of only four π pulses, but it required different T^{PASS}'s for different Θ's. This would result in different T_2 decays (first term in Eq. [9]) for the different Θ increments and consequently to an additional intensity modulation, which will spoil the 2D experiment. The modification of the original four-pulse sequence (*20*) to a five-pulse sequence (*24*) is thus crucial in making the 2D-PASS experiment work at all.

As an example of the PASS performance we show in Fig. 3 the MAS spectrum of DMS (a) along with its PASS spectrum (b), with well-resolved and well-phased ssb. The spectrum is essentially free of artifacts and exhibits the same relative ssb intensities as the MAS spectrum. In general, the spectrum will consist of several ssb manifolds and a 2D-PASS experiment will allow decomposing them simultaneously according to the ssb order.

To calculate the PATROS spectrum we introduce the tr-ODESSA fid as an input to the PASS experiment. The exchange information comes from the former part, while the latter will separate the ssb according to their order. Combining Eqs. [3] and [8], and again taking the echo combination of the cos and sin signals of the tr-ODESSA sequence, yields

$$M_{ij}^{PATROS}(t) = e^{-((T_R/2)/T_2)} e^{-i\omega_0\sigma^j_{iso}(T_R/2)} f^j(\gamma)\, f^{*j}(\pi + \gamma) \times e^{-((T^{PASS}+t)/T_2)} e^{i\omega_0\sigma^i_{iso}t} f^{*i}(\pi + \omega_R\tau_m + \gamma + \Theta)\, f^i(\pi + \omega_R\tau_m + \omega_R t + \gamma). \quad [10]$$

The end of the first line in Eq. [10] corresponds to the signal at the end of the preparation period, while the second line describes its evolution after the mixing period and the PASS sequence. Note that the only differences between Eq. [10] and Eq. [3] are the constant decay during the PASS sequence and the extra phase shift Θ in the f^{*i} function. To obtain pure absorption spectra, we need to compensate for the extra phases (Θ and π) accumulated during the PASS and the tr-ODESSA sequences. Using a similar approach to that used in the tr-ODESSA experiment (*16*) and the 2D PASS in Ref. (*24*) we achieve this goal by setting the mixing period to

$$\tau_m = (G - \tfrac{1}{2} - \Theta/2\pi)T_R \quad [11]$$

and start the acquisition at $t = T_R/2$, with $t' = t - T_R/2$. Entering these conditions in Eq. [10] and expanding as above, the PATROS signal becomes

$$M_{ij}^{PATROS}(t') = e^{-((T_R+T^{PASS}+t')/T_2)} e^{i\omega_0(\sigma^i_{iso}-\sigma^j_{iso})(T_R/2)} e^{i\omega_0\sigma^i_{iso}t'} \times \sum_N e^{iN\omega_R t'} e^{-iN\Theta} \sum_M (-1)^{(M-N)} I^{ij}_{MN}. \quad [12]$$

A more complete derivation of this equation is given in the Appendix. As in Eq. [5], the overall time-domain signal finally becomes

$$S(t',\, \tau_m) = \sum_{ij} P_{ij}(\tau_m)\, M_{ij}^{PATROS}(t'). \quad [13]$$

The requirement to synchronize τ_m according to Θ (Eq. [11]) implies that for each increment a slightly different mixing period is used. The largest variation in τ_m within one PATROS sequence is a single rotation period. Thus, for long mixing periods (several T_R's) these variations do not introduce a severe error, while for mixing periods short compared to the reaction halftime, the PATROS spectrum should be similar to that of the PASS. The synchronization of the mixing period is, however, crucial for obtaining artifact-free spectra. This is well demonstrated in the DMS PATROS spectra of Figs. 3c and 3d, which were recorded with a mixing periods short compared to

the mean lifetime between π flips (15 ms (*16, 32*)). In Fig. 3c the mixing period was correctly adjusted according to Eq. [11], with $G = 2$, while in Fig. 3d it was intentionally set, incorrectly, to $\tau_m = (G - \frac{1}{2})T_R$ (the tr-ODESSA condition). It may be seen that the spectrum shown in Fig. 3c is indeed very similar to that of the PASS (Fig. 3b), while the spectrum in Fig. 3d is completely corrupted due to the miss setting of the mixing period.

3. EXPERIMENTAL ASPECTS

An important point of the PATROS experiment concerns the phase cycling of both the PASS and tr-ODESSA parts. Proper phase cycling is crucial for creating the correct combination of the cos and sin signals of the tr-ODESSA part, and for suppressing artifacts that may result from the PASS pulse train. The tr-ODESSA sequence requires a minimum cycle of four steps: a cos and a sin experiment, each with phase alternation, to ensure that the signals decay to zero for $\tau_m \gg T_1$ (*16, 33*). The latter is affected by alternating the phase of the initial proton-$\pi/2$ pulse (not shown in Fig. 2) in concert with that of the receiver. The proper (echo) combination of the cos and sin signals is ensured by synchronous 90° shifts of the phases of the 1st ^{13}C-$\pi/2$ pulse and of the receiver:

$$^1\text{H}\text{–}\pi/2 \text{ pulse: } (+x\ -x)^2$$

$$^1\text{H–CP: } (+y)^4$$

$$^{13}\text{C–CP: } (+y)^4$$

$$1\text{st } \pi/2 \text{ pulse: } (-x)^2(+y)^2$$

$$2\text{nd } \pi/2 \text{ pulse: } (+x)^4$$

$$\text{receiver: } 0\ 2\ 3\ 1$$

For the PASS part, an independent cycling of all five π-pulses in increments of 120° (a total of $3^5 = 243$ steps) was suggested by Antzutkin *et al.* (*24*) in order to correct for pulse imperfections. Combining with the minimum tr-ODESSA cycle of four steps would result in the inconveniently large cycle of 972 steps for the PATROS experiment. We therefore reduced the number of the cycling steps of the PASS sequence by incrementing the phases of the π-pulses in steps of 180°. This resulted in $2^5 = 32$ steps for the PASS sequence and a total of 128 steps for the whole PATROS experiment. The spectra shown in Figs. 3b and 3c, which were recorded using this reduced sequence, demonstrate that it indeed produces satisfactory results:

$$^1\text{H}\text{–}\pi/2 \text{ pulse: } (+x\ -x)^{2*32}$$

$$^1\text{H–CP: } (+y)^{4*32}$$

$$^{13}\text{C–CP: } (+y)^{4*32}$$

$$1\text{st } \pi/2 \text{ pulse: } ((-x)^2(+y)^2)^{32}$$

$$2\text{nd } \pi/2 \text{ pulse: } (+x)^{4*32}$$

$$1\text{st } \pi \text{ pulse: } (+y)^{64}(-y)^{64}$$

$$2\text{nd } \pi \text{ pulse: } ((+y)^{32}(-y)^{32})^2$$

$$3\text{rd } \pi \text{ pulse: } ((+y)^{16}(-y)^{16})^4$$

$$4\text{th } \pi \text{ pulse: } ((+y)^8(-y)^8)^8$$

$$5\text{th } \pi \text{ pulse: } ((+y)^4(-y)^4)^{16}$$

$$\text{receiver: } (0\ 2\ 3\ 1)^{32}$$

The performance and sensitivity of the various experiments discussed above, is demonstrated in the MAS, PASS, and PATROS spectra of DMS shown in Fig. 3. All three experiments were made at 25°C with a spinning rate of 1 kHz and 256 scans per spectrum. The signal-to-noise ratio (S/N), measured on the most intense peak ($N = 1$) in the MAS spectrum (Fig. 3a) is about 400. A tr-ODESSA experiment at a short mixing period (not shown) yields a S/N of about 200, as expected because of the separate acquisition of the cos and sin signals. The PASS experiment, with 256 scans for each of the 16 Θ increments and using the timings of the π pulses as given by (*24*) results in a S/N of about 900 (Fig. 3b). Thus, instead of an increase by a factor of four, relative to the MAS, we only find a twofold enhancement in the S/N. The reduction is most probably due to the relaxation losses and pulse imperfections of the PASS part. In the PATROS experiment (Fig. 3c) the S/N is about 300, instead of the expected value of $200 \cdot 4 = 800$. The extra loss is apparently due to the PASS sequence as above.

As another example, in Fig. 4 we compare two spectra obtained from a PATROS experiment on PBMA. The experiment was performed at a MAS frequency of 900 Hz, a very short mixing period corresponding to $G = 2$ (1 to 2 ms), 16 Θ-steps, each with 512 scans. Only the high field (aliphatic) region of the spectrum is shown. The top trace is the FT of the $\Theta = 0$ (1st) increment, while the bottom trace is the $N = 0$ slice of the full 2D experiment. The S/N ratio of the second spectrum is about four times larger than the S/N ratio in the first spectrum, which is consistent with the 16-fold larger number of scans used for the 2D spectrum as compared to that for a single increment. Thus, although PATROS is a more time consuming experiment than the tr-ODESSA, the extra time spent on improving the resolution serves also to improve the sensitivity.

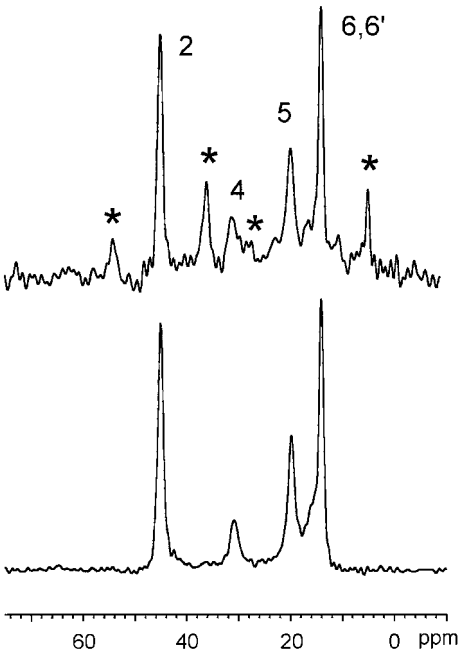

FIG. 4. Carbon-13 PATROS spectra of the aliphatic carbons of PBMA: (bottom) The $N = 0$ slice of the full 2D-spectrum using 16 Θ-increments with 512 scans each; (top) The 1D-FT spectrum of the 1st Θ-increment of the same experiment. The numbers label the center peaks of the observed ssb manifolds and the asterisks indicate a few of the spinning side bands. Note the absence of signals due to carbons 1 and 3; $t = 45°C$, $\nu_R = 900$ Hz.

To extract kinetic parameters from PATROS, the experiment needs to be repeated for several different mixing periods and the ssb intensities analyzed in terms of the exchange rates and the T_1 relaxation. For the most common situation of two-site jumps, Eq. [7] is applicable. As an example, in Fig. 5 we show the results of such an analysis for a PATROS experiment on DMS, where the intensities of the $N = 1$ and $N = 0$ ssb, $I_N^{PATROS}(\tau_m)$, are plotted versus τ_m. The solid symbols in this figure are experimental points, while the curves are best-fit simulations Eq. [7], with $k = 185\ s^{-1}$ and $T_1 = 0.18$ s. Note that the results are plotted in a loglinear (Time–Intensity) scale, where characteristic decay times correspond to centers of dispersion sigmoids. Each curve exhibits two well-pronounced dispersions, with the shorter one (at $\tau_m \sim 2.7$ ms) being due to the molecular π-flips and the longer one (at $\tau_m \sim 180$ ms) reflecting the T_1 relaxation decay.

The NMR experiments were performed on a UNITY INOVA 400 spectrometer using a VARIAN/JAKOBSEN 7-mm VT CPMAS probe (*34*). The entire volume of the rotor was used, i.e., no spaces to restrict the sample to the center of the coil were applied. Constant amplitude CP and CW ^{1}H-decoupling (at $\omega_2/2\pi = 70$ kHz) were applied. Typical pulse widths were 4 μs for both the ^{1}H and ^{13}C channels. Synchronization of the mixing period with the MAS rotation was performed as described in (*35*).

4. ULTRASLOW MOTIONS IN POLY(*n*-BUTYLMETHACRYLATE) (PBMA)

A major interest in polymer sciences is the identification of segmental motions in these molecules and determining their kinetic parameters. For PBMA (see insert in Fig. 1), such separate motions may involve the polymer backbone, the side chains, and the carboxylic linking groups. The latter can readily be studied by tr-ODESSA, because its ssb are well separated from the rest of the peaks in the spectrum (see Fig. 1). Such a study is currently underway and will be reported elsewhere. This method fails, however, for the aliphatic carbons, because of the lack of observed ssb at high spinning rates and the excessive overlap between them at low spinning rates (see bottom and top traces in Fig. 1, corresponding to $\nu_R = 4.9$ and 0.9 kHz, respectively). This situation is an ideal example for the application of the PATROS method. We shall show that using PATROS, it is indeed possible to resolve the ssb according to their order and study separately the mobilities of the polymer backbone and of the aliphatic side chains.

In Fig. 6 are shown the aliphatic regions of two PATROS spectra of PBMA, recorded at $\nu_R = 900$ Hz with nominal mixing periods of 1 ms and 1 s, respectively. Sixteen Θ-increments were recorded (512 scans, each). Only the inner 9 slices are shown. It may be seen that the peaks due to carbons 1 (at 64 ppm) and carbon 3 (at 55 ppm) due, respectively, to main-chain methylene and bridging side-chain methylene are completely absent in the PATROS spectra (cf. Fig. 1). This is almost certainly due to transverse relaxation decay. The overall duration during which T_2 relaxation occurs is two rotation periods (one during the PASS part and another during the tr-ODESSA parts), i.e., 2.22 ms for $\nu_R = 900$ Hz. These lines are significantly broader than the others, with full width at half-maximum height, of 400 Hz for carbon 1 and 650 Hz for carbon 3. If these widths are converted into transverse relaxation, a decay of more than 90% can be expected for both lines.

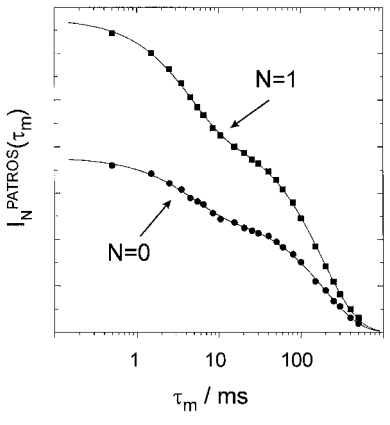

FIG. 5. Plots of the $N = 1$ and $N = 0$ carbon-13 ssb intensities of DMS in a PATROS experiment as a function of the mixing time. The experimental conditions are as in Fig. 3c.

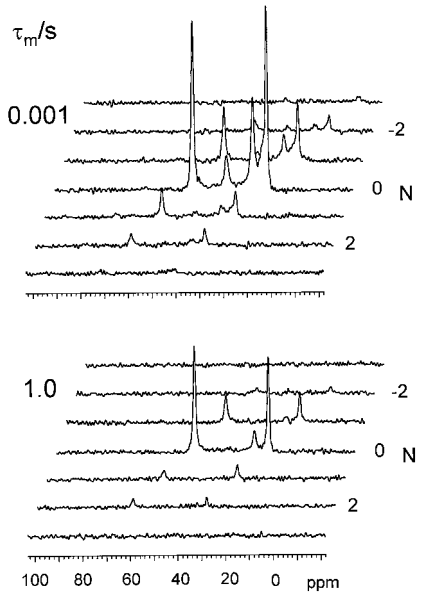

FIG. 6. Carbon-13 PATROS spectra of the aliphatic region of PBMA, for two mixing periods as indicated; $t = 45°C$, $\nu_R = 900$ Hz, recycle time 1.1 s, 16 Θ increments with 512 transients each were accumulated, resulting in an overall measuring time of about 2.5 h for each τ_m.

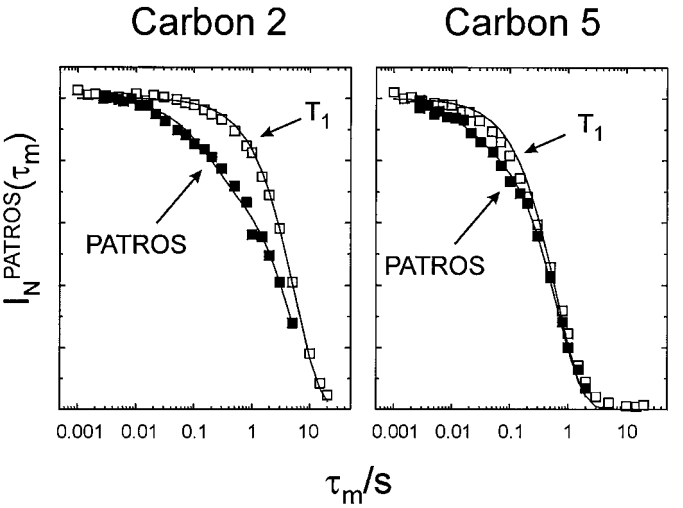

FIG. 7. (solid symbols) The $N = 0$ peak intensities for carbons 2 and 5 of PBMA in PATROS experiments of the type shown in Fig. 6; (open symbols) corresponding results for T_1 inversion-recovery experiments. Experimental conditions as in Fig. 6. The solid curves are best-fit simulations to single exponential decays for the T_1 data and to Eq. [14] for the PATROS data. They were calculated using the parameters given in Table 1.

The line widths of the remaining aliphatic peaks in the spectrum is about 200 Hz, corresponding to a loss of "only" 50% of the intensity.

To investigate the separate motions of the backbone and the side chains, we choose carbon 2 (at 44 ppm) for the former and carbon 5 (at 19 ppm) for the latter. At $\nu_R = 900$ Hz these carbons exhibit a sufficient number of ssb for monitoring dynamic processes. The PATROS intensities of these peaks were measured over a wide range of mixing periods and the results are plotted in the two diagrams of Fig. 7. Also plotted in these diagrams are the T_1 decays of the corresponding peaks as measured by the method of Ref. (*33*). The latter curves were fitted to single exponential decays and yielded T_1 values of 5.5 and 0.66 s for carbons 2 and 5, respectively. The large difference between the two T_1's most likely reflects the higher mobility of the side chain as compared to that of the polymer backbone in the fast motion (relaxation) regime. On the other hand, the PATROS curves clearly show additional dispersions which corresponds to much slower motions, on the time scale of the τ_m's used, i.e., of the order of several milliseconds to several hundred milliseconds. We have accordingly fitted the PATROS results to an equation of type Eq. [7], except that the exponential $\exp(-2k\tau_m)$ was substituted by a stretched exponential function $\exp[-(\tau_m/\tau_c)^{\beta}]$ (*1, 36*),

$$I_N(\tau_m) = (A_N + B_N e^{-(\tau_m/\tau_c)^{\beta}}) e^{-(\tau_m/T_1)}. \qquad [14]$$

The use of stretched exponents implies a distribution of correlation times, which is very often the situation in real polymers (*4*). The parameter β reflects the width of this distribution and τ_c the mean value of the correlation times. In the analysis of the data in terms of Eq. [14], we treated A_N and B_N as free parameters. The final results are summarized in Table 1. The fact that β is close to 1 indicates a narrow distribution of correlation times. However, since the part of the signal, which decays due to exchange, $B_0/(A_0 + B_0)$, is only 10 to 20% of the overall intensity, the determination of β is subject to a large error. On the other hand, the determination of the correlation times, as reflected in the dispersion, is quite accurate. The extra dispersions due to the slow motions fall at $\tau_m = 110$ ms for the main-chain carbon 2 and at $\tau_m = 21$ ms for the side-chain carbon 5. These correlation times correspond to the ultraslow NMR regime. As they are not associated with polar groups, they are difficult to detect and identify by other than exchange NMR methods.

TABLE 1
Parameters Derived by Fitting the T_1- and PATROS-Decay Results of Fig. 7 for Carbons 2 and 5 to Eq. [14]

	Carbon 2	Carbon 5
T_1/s[a]	5.5	0.66
T_1/s[b]	5.0	0.66
A_0	0.8	0.89
B_0	0.2	0.11
τ_c/s	0.11	0.021
β	0.9	0.9

[a] Obtained from an independent T_1 experiment.
[b] Obtained from the PATROS experiment.

It should be emphasized that while the results clearly indicate the presence of ultraslow motions in the main and side chains of the PBMA polymer, they do not report on the mechanism of the motion. In principle, such information could be derived by accurate measurements of the A_N's and B_N's in Eq. [14], but for the present system it does not appear practical.

It may be noted (Table 1 and Fig. 7) that for the side-chain methylene (carbon 5), the T_1 determined by inversion recovery (*33*) and by the PATROS experiments are identical (0.66 s), while for the main-chain methylene (carbon 2), the T_1 derived from PATROS is slightly shorter than that determined directly (5.0 versus 5.5 s). We believe that the difference is real and reflects a small contribution from spin diffusion kinetics (*18*), which was neglected in the analysis. The long mixing periods required to monitor the slowly decaying signal due to carbon 2 reaches the range where spin diffusion effects in natural abundance carbon-13 become detectable (*18, 30, 37*).

5. SUMMARY AND CONCLUSION

We have introduced a modified version of the tr-ODESSA experiment for measuring slow exchange processes in situations where there is overlap between ssb of inequivalent carbons. The method consists of a hybrid of the tr-ODESSA and the PASS sequence. The latter serves to separate, in a second dimension, the ssb according to their order and thus remove the overlap between them. The method is particularly applicable to situations where there are a number of inequivalent carbons with small chemical shift anisotropies. In such cases it is necessary to apply slow spinning and as a result, there is excessive overlap between ssb of different nuclei. The PATROS method removes this overlap and allows accurate intensity measurement of different ssb as a function of the mixing period. Such situations often occur in systems containing aliphatic chains, as in synthetic polymers, detergents, and liquid crystals. We have demonstrated the applicability of the method to monitor ultraslow motions in PBMA. It is important to note, however, that for broad lines (in particular for slow spinning), there is a substantial loss of intensity due to T_2 relaxation. This limits the method to signals with relatively narrow lines.

The original idea of the tr-ODESSA was to substitute the 2D-exchange experiment by a 1D method. The PATROS experiment seems as a turn-back, as it is a kind of 2D-experiment. In fact it is a highly reduced version of 2D exchange as it requires only as many increments, in the indirect dimension, as the number of observed ssb. Also, since there is no signal decay in the indirect dimension, the S/N of the PATROS is, in principle, identical to that of the tr-ODESSA (per scan). In practice, however, there is signal loss due to transverse relaxation and accumulated pulse imperfections during the PASS part of the experiment. The main advantage of the PATROS is in resolving the overlap between ssb belonging to inequivalent carbons. Such overlaps are not resolved in the normal 2D-MAS exchange experiments. This is demonstrated for the case $\nu_R \approx |\nu^a_{iso} - \nu^b_{iso}|$ schematically in Fig. 8, where a contour plot of a 2D-exchange spectrum for two interchanging ssb manifolds is compared with a stack plot of a corresponding 2D PATROS spectrum: while in the 2D-MAS spectrum the most intensive cross peaks belonging to different carbons still suffer from overlap, all ssb are well separated in the PATROS spectrum.

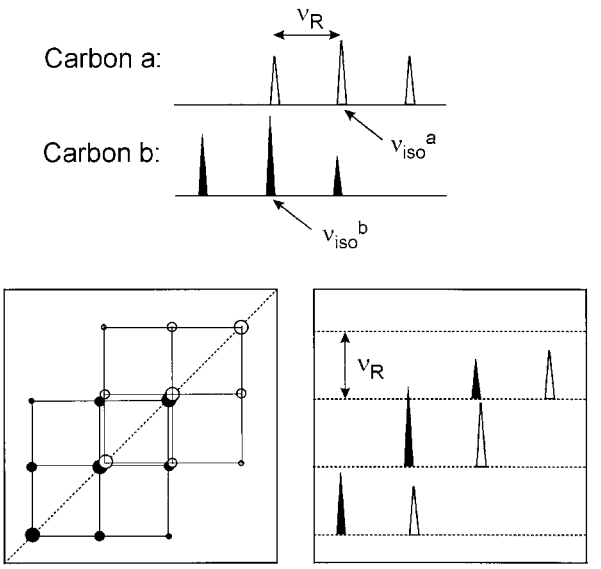

FIG. 8. Schematic presentation of two types of 2D MAS spectra consisting of two manifolds of exchanging carbons, C_a and C_b (top). (left) A contour plot of a rotor-synchronized 2D-exchange spectrum; (right) a stack plot of a 2D-PATROS spectrum. Two families of ssb with ν_R of the order of the isotropic chemical shift difference between them are assumed.

One can think of alternative approaches to eliminate the overlap between the ssb by using other combinations of sequences. For example, instead of the tr-ODESSA/PASS hybrid a EIS/PASS combination can be employed, but we think that the EIS sequence is much less robust to pulse imperfections than the tr-ODESSA. Alternatively the tr-ODESSA could be combined with a TOSS/inverse-TOSS sequence (*38*), which results in separation of the ssb manifolds according to their isotropic chemical shift (in the indirect dimension). This amounts, however, to a full 2D experiment that requires many t_1 increments in order to obtain the desired resolution of the isotropic chemical shift manifolds and does not have the advantage of periodicity in the indirect dimension.

Another sequence that fulfills the requirement of periodicity in the indirect dimension is a sequence suggested by Spiess and co-workers (*22*), which utilizes two TOSS sequences (*21, 39*). It gives a similar spectrum to that of the PASS method, but it is less efficient than the latter since it requires the combination of two separate experiments and thus discards 50% of the signal, it needs twice as many pulses, and it suffers from a larger T_2 decay.

APPENDIX

In this appendix, we present the derivation of Eq. [12] from Eq. [10]

$$M_{ij}^{PATROS}(t) = e^{-((T_R/2)/T_2)} e^{-i\omega_0\sigma_{iso}^j(T_R/2)} f^j(\gamma)\, f^{*j}(\pi+\gamma) \times e^{-((T^{PASS}+t)/T_2)} e^{i\omega_0\sigma_{iso}^i t} f^{*i}(\pi+\omega_R\tau_m+\gamma+\Theta)\, f^i(\pi+\omega_R\tau_m+\omega_R t+\gamma). \quad [A1]$$

As in the tr-ODESSA, we need to reverse the evolution of the isotropic chemical shift during the preparation period. To do so, we (i) start the acquisition at $T_R/2$ after the read-out pulse, (ii) redefine the acquisition time as $t' = t - T_R/2$, and (iii) take the echo combination of the cos and sin signals. The latter is already implied in the tr-ODESSA part of Eq. [A1]. Substituting $t = T_R/2 + t'$ ($\omega_R t = \pi + \omega_R t'$) yields

$$M_{ij}^{PATROS}(t') = e^{-((T_R+T^{PASS}+t')/T_2)} e^{i\omega_0(\sigma_{iso}^i-\sigma_{iso}^j)(T_R/2)} \times f^j(\gamma)\, f^{*j}(\pi+\gamma) e^{i\omega_0\sigma_{iso}^i t'} \times f^{*i}(\pi+\omega_R\tau_m+\gamma+\Theta) \times f^i(\pi+\omega_R\tau_m+\omega_R t'+\gamma+\pi). \quad [A2]$$

In order to maintain the phase of the argument of the f function at the end of the evolution period and at the beginning of the acquisition, we need to (iv) set $\tau_m = (G - \frac{1}{2} - \Theta/2\pi)T_R$, so that $\omega_R\tau_m = 2\pi G - \pi - \Theta$:

$$M_{ij}^{PATROS}(t') = e^{-((T_R+T^{PASS}+t')/T_2)} e^{i\omega_0(\sigma_{iso}^i-\sigma_{iso}^j)(T_R/2)} e^{i\omega_0\sigma_{iso}^i t'} \times f^j(\gamma)\, f^{*j}(\pi+\gamma)\, f^{*i}(\gamma) \times f^i(\gamma-\Theta+\omega_R t'+\pi). \quad [A3]$$

To arrange the f functions in a convenient order, we substitute $\gamma' = \gamma + \pi$:

$$M_{ij}^{PATROS}(t') = e^{-((T_R+T^{PASS}+t')/T_2)} e^{i\omega_0(\sigma_{iso}^i-\sigma_{iso}^j)(T_R/2)} e^{i\omega_0\sigma_{iso}^i t'} \times f^{*j}(\gamma')\, f^j(\gamma'-\pi)\, f^{*i}(\gamma'-\pi) \times f^i(\gamma'-\Theta+\omega_R t'). \quad [A4]$$

Introducing δ-functions (*28*) and expanding yields

$$\begin{aligned} M_{ij}^{PATROS}(t') &= e^{-((T_R+T^{PASS}+t')/T_2)} e^{i\omega_0(\sigma_{iso}^i-\sigma_{iso}^j)(T_R/2)} e^{i\omega_0\sigma_{iso}^i t'} f^{*j}(\gamma') \\ &\quad \times \int d\vartheta\, \delta(\vartheta-\gamma'+\pi)\, f^j(\vartheta)\, f^{*i}(\vartheta) \\ &\quad \times \int d\phi\, \delta(\phi-\vartheta-\pi+\Theta-\omega_R t')\, f^i(\phi) \\ &= e^{-(T_R+T^{PASS}+t'/T_2)} e^{i\omega_0(\sigma_{iso}^i-\sigma_{iso}^j)(T_R/2)} e^{i\omega_0\sigma_{iso}^i t'} f^{*j}(\gamma') \\ &\quad \times \int d\vartheta \sum_M e^{-iM\vartheta} e^{iM\gamma'} e^{-iM\pi} f^j(\vartheta)\, f^{*i}(\vartheta) \\ &\quad \times \int d\phi \sum_N e^{-iN\phi} e^{iN\vartheta} e^{iN\pi} e^{-iN\Theta} e^{iN\omega_R t'} f^i(\phi). \end{aligned} \quad [A5]$$

Finally, integration over α, β, and γ' and recalling that $e^{-i\pi(M-N)} = (-1)^{(M-N)}$, yields

$$M_{ij}^{PATROS}(t') = e^{-((T_R+T^{PASS}+t')/T_2)} e^{i\omega_0(\sigma_{iso}^i-\sigma_{iso}^j)(T_R/2)} e^{i\omega_0\sigma_{iso}^i t'} \times \sum_N e^{iN\omega_R t'} e^{-iN\Theta} \sum_M (-1)^{(M-N)} I_{MN}^{ij}, \quad [A6]$$

where

$$I_{MN}^{ij} = \int d\alpha \int \sin\beta\, d\beta \int d\gamma' e^{iM\gamma'} f^{*j}(\gamma') \times \int d\phi e^{-iN\phi} f^i(\phi) \int d\vartheta e^{-i(M-N)\vartheta} f^j(\vartheta)\, f^{*i}(\vartheta). \quad [A7]$$

ACKNOWLEDGMENTS

The financial support of the Deutsche Forschungsgemeinschaft DFG (SFB 418), the Fonds der Chemischen Industrie, the German-Israel Foundation, G.I.F. (Research Grant I-558-218.05/97), and the G.M.J. Schmidt Center on Supramolecular Architectures is gratefully acknowledged. We thank Professor Christian Jäger (Jena, Germany) for helpful discussions.

REFERENCES

1. K. Schmidt-Rohr and H. W. Spiess, "Multidimensional Solid-State NMR and Polymers," Chap. 7, Academic Press, London (1994).
2. W. Domberger, D. Reichert, F. Garwe, H. Schneider, and E. Donth, Relaxation behavior in the α splitting region of the glass transition in PnBMA by means of 13C 2D-MAS exchange NMR, *J. Phys. Condens. Matter* **7,** 7419–7426 (1995).
3. G. B. McKenna, Dynamics and mechanics below the glass transi-

tion: The non-equilibrium state, *Comput. Mater. Sci.* **4,** 349–360 (1995).

4. E. J. Donth, "Relaxation and Thermodynamics in Polymers: Glass Transition," Akademie Verlag, Berlin (1992).
5. T. M. Connor, B. E. Read, and G. Williams, Dielectric, dynamic mechanical and nuclear resonance properties of polyethylene oxide as a function of molecular weight, *J. Appl. Chem.* **14,** 74–81 (1964).
6. M. Wilhelm and H. W. Spiess, Detection of slow 180° phenylene flips in PET fibres via ^{13}C two-dimensional solid-state exchange NMR, *Macromolecules* **29,** 1088–1090 (1996).
7. A. G. Palmer, J. Williams, and A. McDermott, Nuclear magnetic resonance studies of biopolymer dynamics, *J. Phys. Chem.* **100,** 13,293–13,310 (1996).
8. A. Krushelnitsky, D. Reichert, G. Hempel, V. Fetodov, H. Schneider, L. Yagodina, and A. Shulga, Superslow backbone protein dynamics as studied by 1D solid-state MAS exchange NMR spectroscopy, *J. Magn. Reson.* **138,** 244–255 (1999).
9. A. P. M. Kentgens, A. F. de Jong, and W. S. Veeman, A 2D-exchange NMR study of very slow molecular motions in crystalline poly(oxymethylene), *Macromolecules* **18,** 1045–1048 (1985).
10. A. P. M. Kentgens, E. de Boer, and W. S. Veeman, Ultraslow molecular motions in crystalline polyoxymethylene. A complete elucidation using two-dimensional solid state NMR, *J. Chem. Phys.* **87,** 6859–6866 (1987).
11. A. Hagemeyer, K. Schmidt-Rohr, and H. W. Spiess, Two-dimensional magnetic resonance experiments for studying molecular order and dynamics in static and rotating solids, *Adv. Magn. Reson.* **13,** 85–130 (1989).
12. N. M. Szeverenyi, A. Bax, and G. E. Maciel, Proton-exchange rates in solid tropolone as measured via ^{13}C-CP/MAS NMR, *J. Am. Chem. Soc.* **105,** 2579–2582 (1983).
13. C. Connor, A. Naito, K. Takegoshi, and C. A. McDowell, Intermolecular spin-diffusion between ^{31}P nuclei in a single crystal of dipotassium α-D-glucose-1-phosphate dihydrate; a 1-D analogue of the 2-D exchange NMR experiment, *Chem. Phys. Lett.* **113,** 123–128 (1985).
14. Y. Yang, M. Schuster, B. Blümich, and H. W. Spiess, Dynamic magic-angle spinning NMR spectroscopy: Exchange induced spinning sidebands, *J. Magn. Reson.* **139,** 239–243 (1987).
15. V. Gerardy-Mountouillout, C. Malveau, P. Tekely, Z. Olender, and Z. Luz, Odessa-A new 1D-exchange experiment for chemically equivalent nuclei in rotating solids, *J. Magn. Reson. A* **123,** 7–15 (1996).
16. D. Reichert, H. Zimmermann, P. Tekely, R. Poupko, and Z. Luz, Time-reverse Odessa. A 1D Exchange experiment for rotating solids with several groups of equivalent nuclei, *J. Magn. Reson.* **125,** 245–258 (1997).
17. P. Tekely, D. Reichert, H. Zimmermann, and Z. Luz, Initial conditions for ^{13}C MAS NMR 1D exchange involving chemically equivalent and inequivalent nuclei, *J. Magn. Reson.,* in press.
18. D. Reichert, G. Hempel, R. Poupko, Z. Luz, Z. Olejniczak, and P. Tekely, Carbon-13 spin exchange in durene as studied by MAS spectroscopy, *Solid State NMR* **13,** 137–148 (1998).
19. D. Reichert, G. Hempel, H. Zimmermann, P. Tekely, R. Poupko, Z. Luz, D. E. Favre, and B. F. Chmelka, The dynamics of aromatic ring flips in solid 4,4′-diphenoxydiphenylether as studied by carbon-13 trODESSA NMR, *Appl. Magn. Reson.* **17,** 315–327 (1999).
20. W. T. Dixon, Spinning-sideband-free and spinning-sideband-only NMR spectra in spinning samples, *J. Chem. Phys.* **77,** 1800–1809 (1982).
21. W. T. Dixon, Spinning-sideband-free NMR spectra, *J. Magn. Reson.* **44,** 220–223 (1981).
22. S. F. DeLacroix, J. J. Titmann, A. Hagemeyer, and H. W. Spiess, Increased resolution in MAS NMR spectra by two-dimensional separation of sidebands by order, *J. Magn. Reson.* **97,** 435–443 (1992).
23. J. J. Titmann, S. F. DeLacroix, A. Hagemeyer, and H. W. Spiess, Structure and order in partially oriented solids by three-dimensional magic angle spinning nuclear magnetic resonance spectroscopy. *J. Chem. Phys.* **98,** 3816–3826 (1993).
24. O. N. Antzutkin, S. C. Shekar, and M. H. Levitt, Two-dimensional sideband separation in magic-angle spinning NMR, *J. Magn. Reson. A* **115,** 7–19 (1995).
25. O. N. Antzutkin, Y. K. Lee, and M. H. Levitt, ^{13}C and ^{15}N chemical shift anisotropy of ampicillin and penicillin-V studied by 2D-PASS and CP/MAS NMR, *J. Magn. Reson.* **135,** 144–155 (1998).
26. Z. Song, O. N. Antzutkin, A. Rupprecht, and M. H. Levitt, Order-resolved sideband separation in magic-angle-spinning NMR: ^{31}P of oriented DNA fibers, *Chem. Phys. Lett.* **253,** 349–354 (1996).
27. O. N. Antzutkin, Sideband manipulation in magic-angle-spinning nuclear magnetic resonance, *Prog. Nucl. Magn. Reson. Spectrosc.* **35,** 203–266 (1999).
28. M. Mehring, High-resolution NMR in solids, *in* "NMR-Basic Principles and Progress," Vol. 11, Springer, Berlin (1976).
29. Z. Luz, H. W. Spiess, and J. J. Titman, Rotor synchronized MAS two-dimensional exchange NMR in solids. Principles and applications, *Isr. J. Chem.* **32,** 145–160 (1992).
30. Z. Olender, D. Reichert, A. Müller, H. Zimmermann, R. Poupko, and Z. Luz, Carbon-13 chemical-shift correlation, spin-diffusion and self diffusion in isotopically enriched tropolone, *J. Magn. Reson. A* **120,** 31–45 (1996).
31. J. Herzfeld and A. E. Berger, Sideband intensities in NMR spectra of sample spinning at the magic angle, *J. Chem. Phys.* **73,** 6021–6030 (1980).
32. M. J. Brown, R. L. Vold, and G. L. Hoatson, Selective inversion investigations of slow molecular motion in solid state deuteron NMR spectroscopy, *Solid State NMR* **6,** 167–185 (1996).
33. D. A. Torchia, The measurement of proton-enhanced carbon-13 T_1 values by a method which suppresses artifacts, *J. Magn. Reson.* **30,** 613–616 (1978).
34. H. J. Jakobsen, P. Daugaard, and V. Langer, CP/MAS NMR at high speeds and high fields, *J. Magn. Reson.* **76,** 162–168 (1988).
35. D. Reichert, G. Hempel, and H. Schneider, Experimental artifacts in 2D-MAS exchange experiments: Non-uniform mixing time within a single 2D run, *Solid State NMR* **11,** 259–265 (1998).
36. G. Williams and D. C. Watts, Non-symmetrical dielectric relaxation behavior arising from a simple empirical decay function, *Trans. Faraday Soc.* **66,** 80–85 (1970).
37. D. L. Vanderhard, Natural-abundance ^{13}C–^{13}C spin exchange in rigid crystalline organic solids, *J. Magn. Reson.* **72,** 13–47 (1987).
38. A. C. Kolbert and R. G. Griffin, Two-dimensional resolution of isotropic and anisotropic chemical shift in magic angle spinning NMR, *J. Chem. Phys.* **166,** 87–91 (1990).
39. W. T. Dixon, J. Schaefer, M. D. Sefcik, E. O. Stejskal, and R. A. McKay, Total suppression of side bands in CPMAS C-13 NMR, *J. Magn. Reson.* **49,** 341–345 (1982).